JOURNAL OF MATERIALS SCIENCE 23 (1988) 1615–1631

# Fractography of unfilled and particulate-filled epoxy resins

W. J. CANTWELL, A. C. ROULIN-MOLONEY
*Laboratoire de Polymères, Ecole Polytechnique Fédérale de Lausanne, 32 ch. de Bellerive, CH-1007 Lausanne, Switzerland*

T. KAISER
*ASEA-Brown Boveri Ltd., Corporate Research, CH-5405 Baden, Switzerland*

The objective of this work was to analyse and understand the types of fracture surface morphology found in unfilled and particulate-filled epoxy resins in the light of the thermomechanical history of the specimen (loading rate or duration of loading, temperature, strain at break). Short-term tensile tests and long-term creep tests were conducted at four different temperatures. The fracture surface features were analysed using the scanning electron and optical microscopes and, where suitable, an image analyser. In order to correlate these morphologies with certain regimes of crack velocity, fracture mechanics tests were also conducted, varying the crack speed between $10^{-7}$ and $10^{2}$ m sec$^{-1}$. In the case of the filled resin, the lifetime under static loading is governed by a phase of slow, sub-critical crack growth which is manifested by resin–particle debonding. Thereafter, the crack accelerates and finally may reach terminal velocities depending on the amount of stored elastic energy available at the moment of fracture.

## 1. Introduction

Highly crosslinked polymers such as epoxy resins are ideally suited for a wide range of applications such as matrices in reinforced composites, adhesives in the aerospace industry and as resins for insulating materials used in the power industry. As a result of these demands, much work has been undertaken in an attempt to characterize the mechanics of deformation and fracture in these materials over the wide range of loading conditions and environments likely to be encountered in operational service. However, much of this work gives the appearance of being *ad hoc* in nature, and in spite of the fact that many parameters have been varied a deeper understanding of the basic mechanisms still remains a pressing requirement.

With the continued improvement in both low- and high-magnification microscopy techniques, a new generation of sometimes weird and wonderful terms has evolved to describe features apparent on the fracture surfaces of polymeric materials: mist, welts, shards and shish-kebab being typical examples [1–5]. Investigators have frequently sought to explain the formation of these features in terms of critical crack velocities, stress intensity factors, local stress deviations, energy release rates as well as the myriad of material mechanical properties. However, at present the situation remains rather confused.

There is considerable interest in the potential of multiphase systems such as particulate-filled resins where considerable increases in toughness can be achieved without any loss in tensile or flexural strength. Here, too, a thorough understanding of the mechanisms responsible for fracture has not yet been fully achieved. The work presented in this report details the findings of a research project inaugurated to examine and explain the mechanisms involved in the fracture of a silica-filled epoxy resin under a variety of test conditions. Since short-term tests do not fully represent those encountered in operational service, an extensive programme of creep tests encompassing a wide range of temperatures has been undertaken. With the aid of both scanning electron and optical microscopes attention has been given to identifying and explaining those features and regions apparent on the fracture surface of this filled epoxy resin, with the aim of developing new systems with enhanced static fatigue capability.

## 2. Experimental procedure

### 2.1. Materials and specimen preparation

The resin used in this investigation was a hydantoin-based epoxy resin (Type XB 2900 from Ciba Geigy) cured by a formulated anhydride hardener, HY 925, also from Ciba Geigy. The resin was used both in the unfilled state and filled with silica particles (mean size of approximately 50 $\mu$m) to give a volume fraction of 40%. In order to avoid machining, the resin was generally cured in individual pre-heated moulds. The curing was carried out in accordance with the manufacturer's instructions, that is, a gelation time of 4 h at 80° C followed by 16 h at 130° C. This procedure yielded a uniform distribution of particles and a material with a glass transition temperature of 120° C.

### 2.2. Test specimen details

In order to reproduce the loading conditions likely to

0022–2461/88 $03.00 + .12 

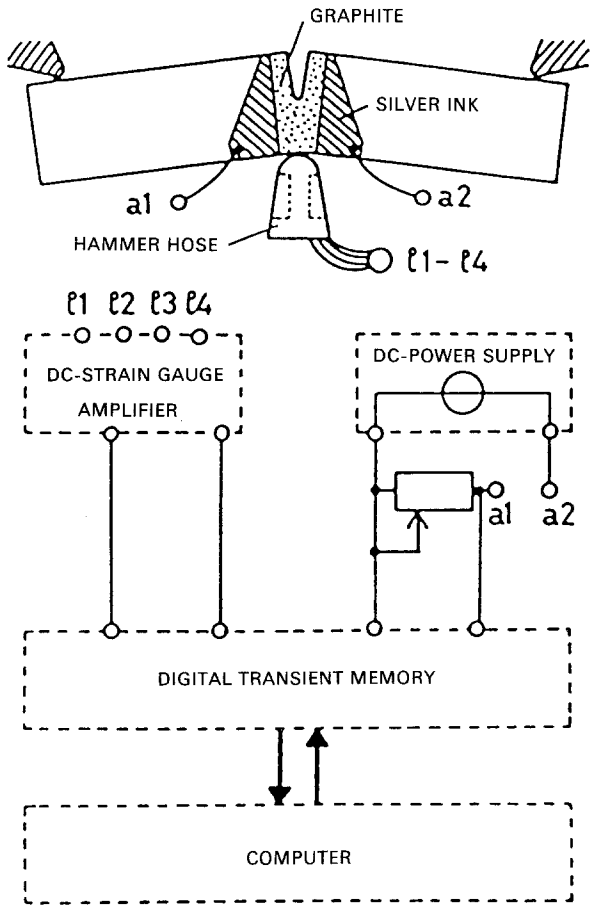


*Figure 1* The graphite gauge as applied to an impact specimen.

be encountered in service, a variety of specimen geometries has been considered, and a brief description of each is given below. Since many of these geometries are inherently unstable the determination of crack velocity by visual observation was impossible. In cases where the geometry permitted, the graphite gauge technique was employed enabling crack velocities up to many hundreds of metres per second to be determined accurately. The method has been described in detail by Stalder *et al.* [6]. It consists of applying a thin layer of graphite to the specimen, bounded by two silver electrodes in the presumed path of the crack. The change in the inverse of resistance with time enables the crack position, and hence the crack velocity, to be determined. The output from the graphite gauge is fed into a data logger TMP30 (W/W Instruments, Switzerland) (capable of enregistering data points up to each 500 nsec) and this is in turn coupled to a Hewlett Packard minicomputer. Fig. 1 gives a schematic diagram of the experimental set-up. This example is for an impact specimen where one channel of the data logger is used for the graphite gauge and the second channel for the output of the strain gauges bonded to the striker. In this manner a simultaneous record of load and the crack position is obtained.

### 2.2.1. The dumb-bell specimen

This specimen geometry (Fig. 2a) was favoured for the majority of the tensile tests since its circular cross-section contained no inherent stress concentrations, effects which were found to give pessimistic failure stresses during preliminary tests on rectangular specimens. Loading was applied through the two specimen ends, giving a nominally uniform distribution of stresses throughout the test length. One drawback of this specimen is that it does not facilitate the use of graphite gauge for velocity determination.

### 2.2.2. Double-torsion geometry

The advantage of the double-torsion test (Fig. 2b) is that the specimen compliance varies linearly with increasing crack length; thus the stress intensity factor is independent of the crack length. For tests at constant displacement rate, the crack velocity is also essentially constant throughout the test. This inherently stable geometry is thus ideally suited for obtaining low crack velocities (typically between $10^{-7}$ and $10^{-1}$ m sec$^{-1}$).

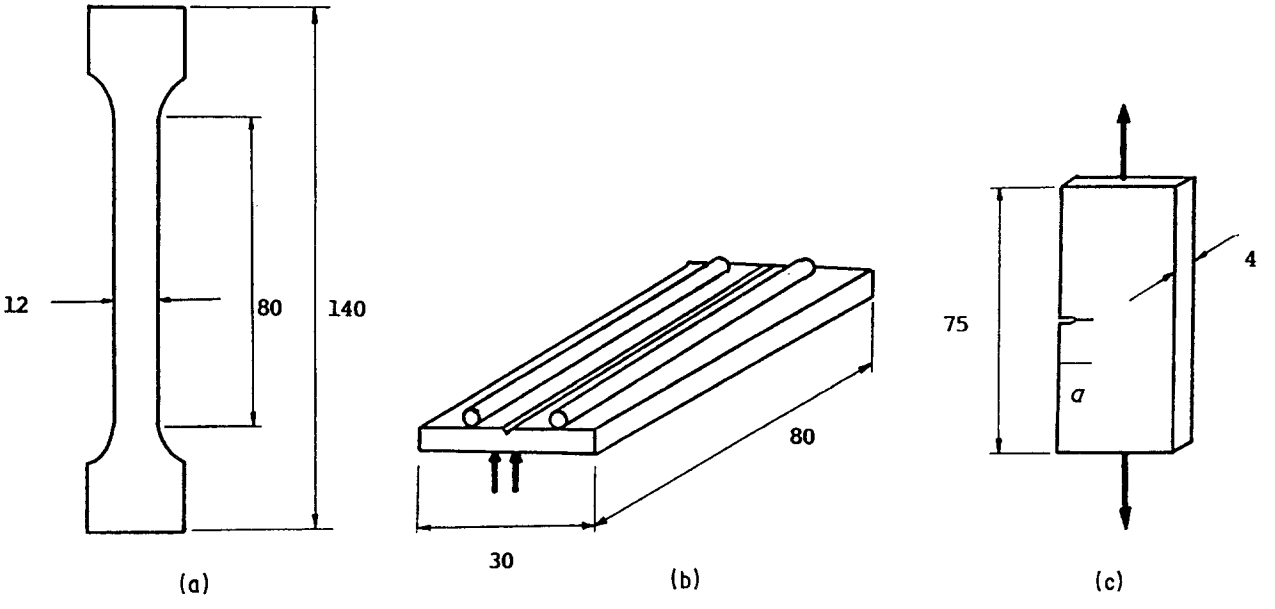


*Figure 2* Specimen geometries used in the fracture tests: (a) standard tensile specimen, (b) double-torsion specimen, (c) single-edge-notch specimen. Dimensions in mm.

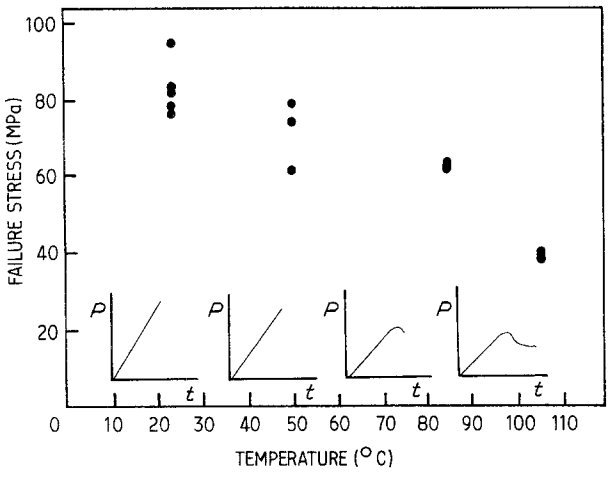


*Figure 3* The variation of failure stress with temperature for the unfilled epoxy.

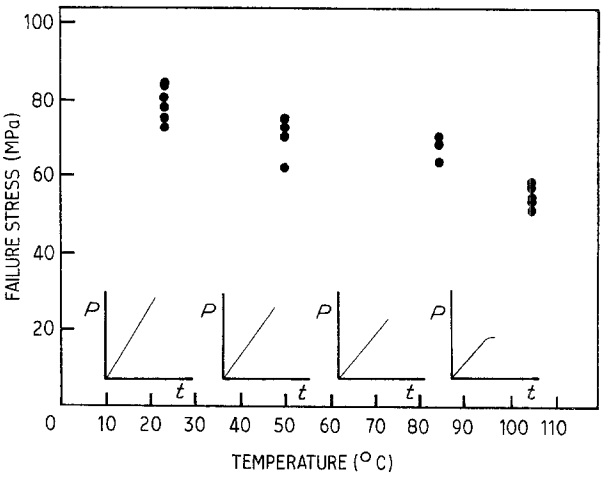


*Figure 4* The variation of failure stress with temperature for the filled epoxy.

### *2.2.3. Single-edge-notch geometry*

The single-edge-notch (SEN) specimen (Fig. 2c) coupled with the graphite gauge technique is an ideal geometry for monitoring rapid crack propagation in polymeric materials. However, great care needs to be taken to assure that the sharpness of the crack meets the requirements for valid $K_{Ic}$ determination. Here, cracks were introduced by applying a controlled pressure to a very sharp razor blade.

## 2.3. Test conditions

### *2.3.1. Short-term tests*

Short-term testing was conducted using an Instron 1122 and a Zwick 1484 universal testing machine. The design of these machines enabled the use of air-circulating ovens when necessary. Testing was conducted at four temperatures: 23, 50, 85 and 105° C. The lower three temperatures represent the range of conditions likely to be found in the operational service of high- and medium-voltage insulators. In order to ensure complete thermal equilibrium, each test specimen was left for approximately 30 min at the required test temperature before testing. For purposes of continuity, most tests were conducted at a crosshead speed of 0.5 mm $min^{-1}$.

### *2.3.2. Long-term tests*

All creep testing was undertaken using the dumb-bell specimen discussed previously. Loading was effected by means of a system of bars and levers which augmented the static load (usually lead weights) by a factor of 10, enabling high stresses to be achieved in the specimen with a minimum of danger. Testing was conducted at four load levels, namely, 20, 40, 60 and 80% of the ultimate strength as determined from the short-term tests. The specimens were supported in four ovens, each of which were capable of accommodating between 7 and 15 independent tests. As before, four test temperatures were considered, (23, 50, 85 and 105° C), permitting comparisons to be made between these tests and the short-term tests discussed above. During the course of the testing, the deformation of the specimen was monitored using an HBM (HBM, West Germany) LY43 strain gauge bonded to the test length. The output was fed into a HBM UPM60 data logger which was in turn coupled to a Hewlett Packard 9300 minicomputer for assessment and subsequent storage of the strain measurements. This system was capable of handling up to 60 separate channels of information once every 2 sec, permitting the complete deformation and failure history of each of the specimens to be recorded accurately.

## 2.4. Fractographic analysis

The resulting fracture surfaces were examined using a low-power Olympus optical microscope and a Cambridge Instruments S100 scanning electron microscope.

# 3. Results and discussion

## 3.1 Mechanical properties

The basic mechanical properties of both the filled and unfilled epoxy were determined by conducting tensile tests on the dumb-bell specimens shown in Fig. 2a. These tests were designed to measure the initial strength of the materials and this value was taken from the maximum point in the load–time curve.

### *3.1.1. Effect of test temperature*

The effect of temperature on the initial strength of the unfilled and filled systems is shown in Figs 3 and 4, respectively. A comparison of the figures indicates that at room temperature the pure epoxy exhibits a slightly superior strength to its silica-filled counterpart; this is in agreement with work reported elsewhere [7]. At lower temperatures, the scatter in the experimental data tends to be greater, perhaps due to a greater sensitivity to defects and flaws. At elevated temperatures, both systems show reductions in initial tensile strength, this being greater in the pure epoxy. Examination of the corresponding load–time curves indicates that considerable yielding has preceded fracture. At these temperatures the scatter in the data is small, indicating that the ultimate strength is now governed by the yield stress of the material. However, it must be noted that the measured "strength" at these temperatures is rate-sensitive; by employing a faster crosshead speed the two figures could be changed.

The effect of temperature on the elastic modulus has been examined only for the filled epoxy. Fig. 5

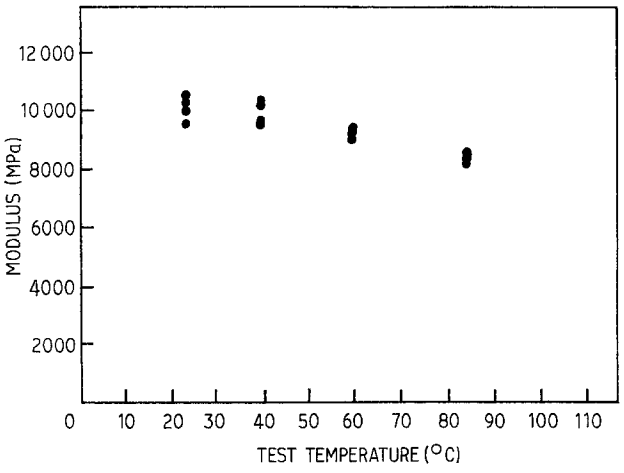


*Figure 5* The variation of modulus with temperature at a crosshead speed of 0.2 mm $min^{-1}$.

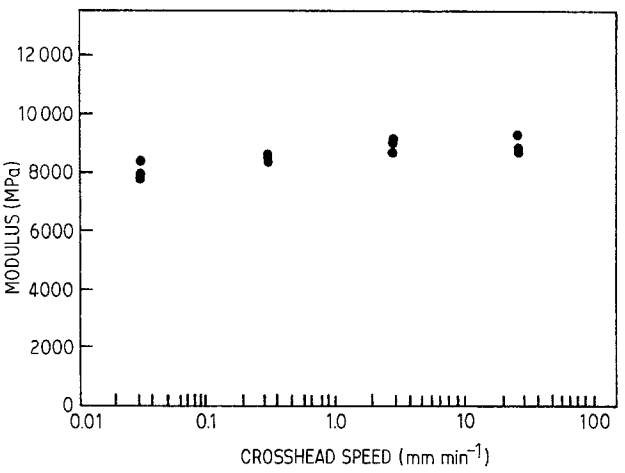


*Figure 7* The variance of modulus with crosshead speed at 85° C.

shows the variation in Young's modulus for a crosshead speed of 0.2 mm $min^{-1}$. As the temperature is increased, the greater degree of molecular mobility within the polymer results in a steady reduction in elastic modulus.

### 3.1.2. The effect of loading rate

Since polymeric materials are viscoelastic by nature, the effects induced by increasing test temperature are often analogous to those produced by lowering the rate of test. Fig. 6 shows the effect of loading rate on the initial tensile strength of the filled epoxy resin when tested at 23° C. Here a 10% increase in strength is realized over a range of approximately three decades of loading rate. Similar effects are apparent in the variation of Young's modulus with test rate. In Fig. 7 significant increases are again evident over a few decades of test rate.

## 3.2. Fractographic analysis

The following sections describe the results of fractographic analysis using both the optical and scanning electron microscopes. Initially, the fracture surface morphologies of the unfilled epoxy resin will be considered since evidence gathered from these observations will be useful for explaining some of the features noted in the filled system which will be discussed subsequently.

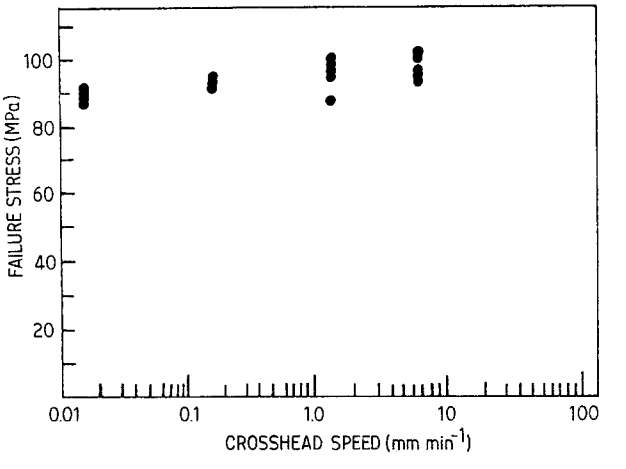


*Figure 6* The variation of tensile strength with crosshead speed at 23° C.

### 3.2.1. The unfilled resin

The appearance of the fractured unfilled resin varied greatly with temperature as demonstrated in the optical micrographs shown in Fig. 8. In each case, fracture initiated in the extreme left of the specimen cross-section. Closer examination of these surfaces highlights a number of regions or zones which are shown schematically in Fig. 9. At the two lower temperatures the initiation points are surrounded by a small semicircular zone frequently termed the mirror region [2]. A detailed scanning electron analysis of these regions indicated that they are, as their name suggests, smooth and featureless. Surrounding this region is a zone characterized by a multitude of small geometric features which are generally parabolic in shape as shown in the left-hand side of Fig. 10a. The occurrence of these markings is almost certainly due to the formation of secondary cracks in the regions of high stress local to the rapidly propagating primary crack. The exact shape of the features depends strongly upon the ratio of the velocities of the primary and secondary cracks. If these velocities are equal, a parabola is formed, whereas if the primary crack is propagating with the greater velocity it will completely enclose the newly formed crack front, yielding an ellipse [1]. Although each of these secondary fractures must contain a defect or flaw, its size was in all cases below the resolving power of the electron microscope and could not therefore be detected. At points further from the origin of fracture these parabolic features interact and overlap, producing more complex geometrical patterns as shown in Fig. 10b. At these low temperatures the remainder of the fracture surface is very rough, indicating that considerable branching of the primary crack has occurred. Examination of the specimen during fracture indicated that the crack velocity in this region is very high, probably some hundreds of metres per second. At 85° C the appearance of the fracture surface changed markedly as shown in Fig. 8c. Here the smooth zone is considerably larger, measuring approximately 4 mm at its maximum point. Closer examination of this region highlights several river markings indicative of cracks propagating on slightly differing planes. In these tests it was possible to observe the crack growing slowly across the specimen until it reached a size comparable

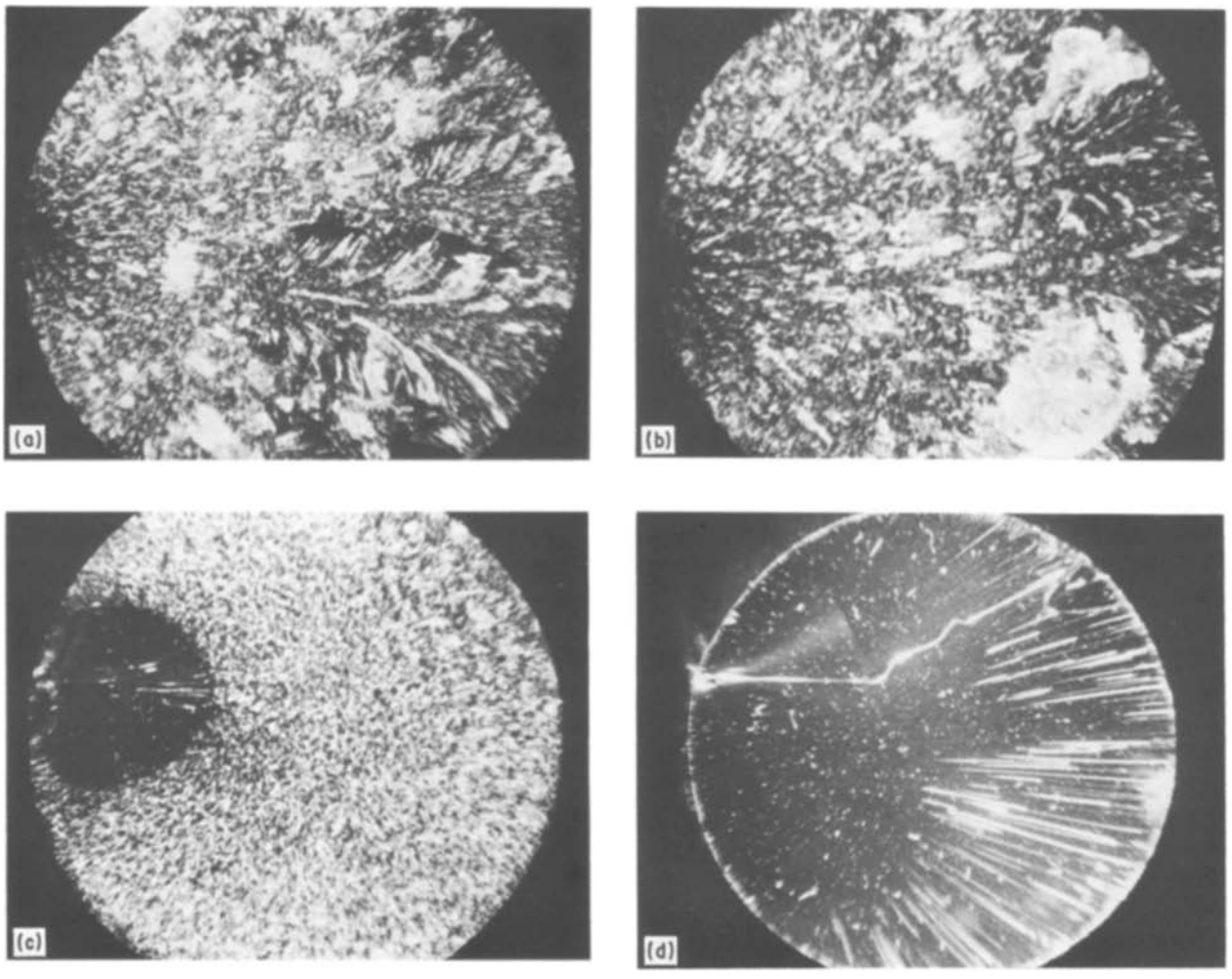


*Figure 8* Fracture surfaces in the unfilled epoxy as a function of temperature: (a) 23° C, (b) 50° C, (c) 85° C, (d) 105° C. × 6.

with that of the mirror zone. It can therefore be stated with confidence that, in this material, the mirror zone represents the region of sub-critical crack growth. The remainder of the fracture surface is almost perfectly flat, displaying only those geometrical patterns discussed above. By 105° C the fracture surface is almost entirely glassy, exhibiting few surface features. In this specimen the failure stress was only 40 MPa, suggesting therefore that the stress system ahead of the crack was sufficient to initiate fracture only from the larger flaws or defects.

In an attempt to quantify some of the effects apparent on the fracture surfaces of the unfilled epoxy system, the size of the mirror zone was determined as

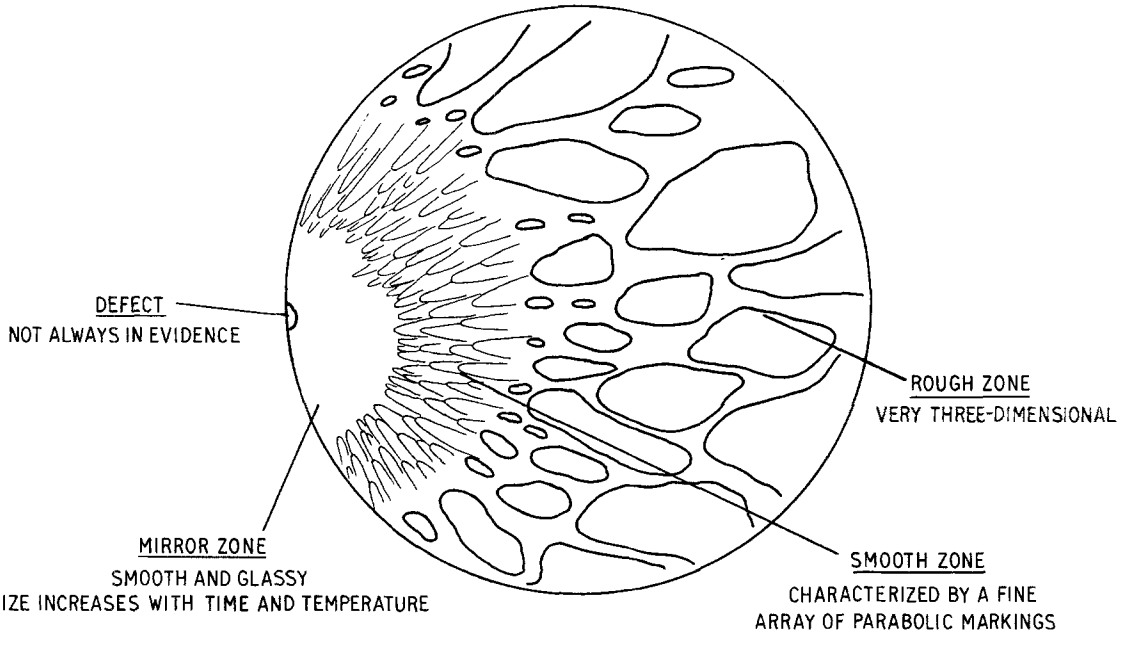


*Figure 9* Regions on the fracture surface in the unfilled epoxy.

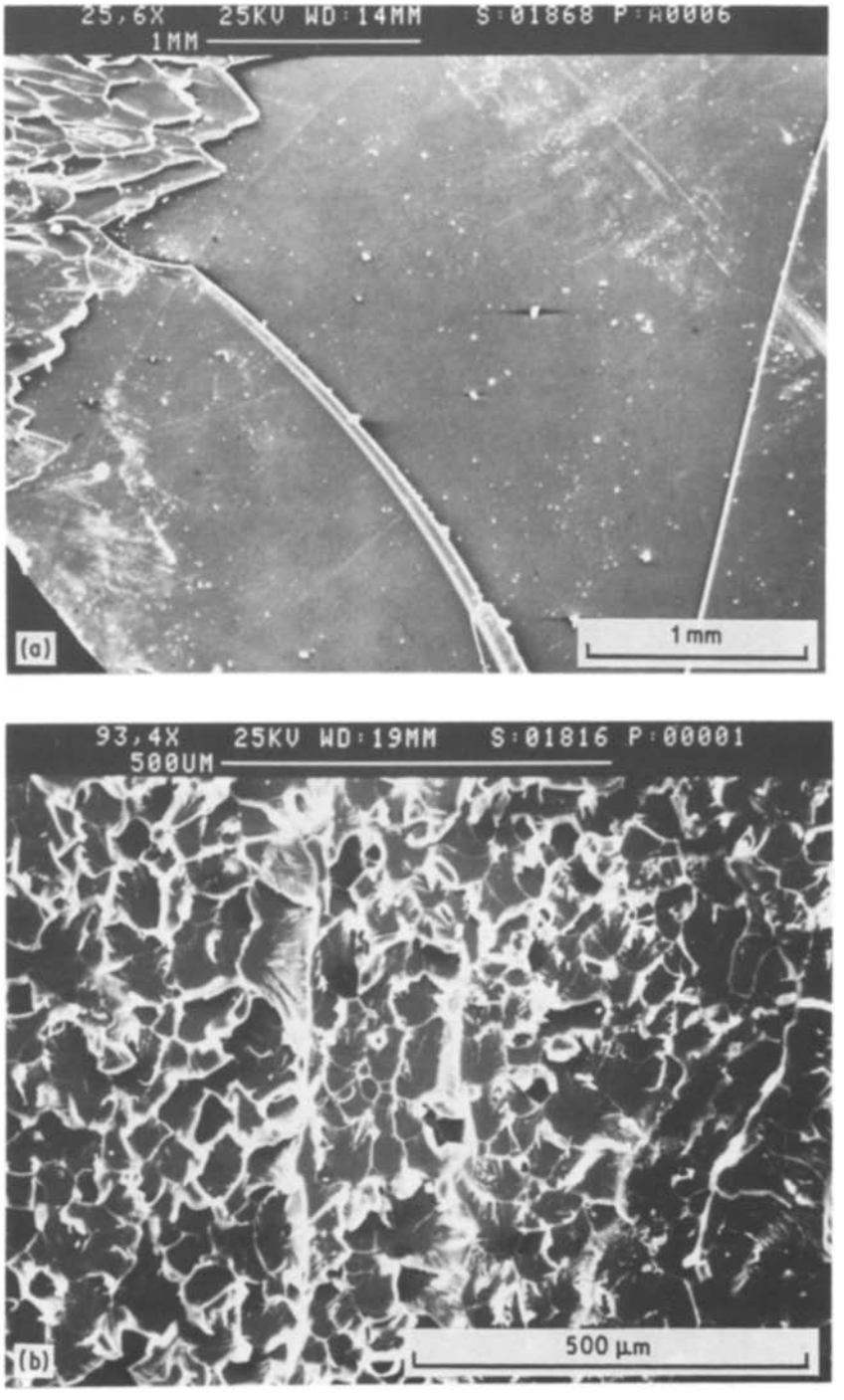


*Figure 10* Scanning electron micrographs showing features on the fracture surface in the unfilled epoxy system: (a) smooth mirror region at high temperature, (b) features on the fast fracture surface.

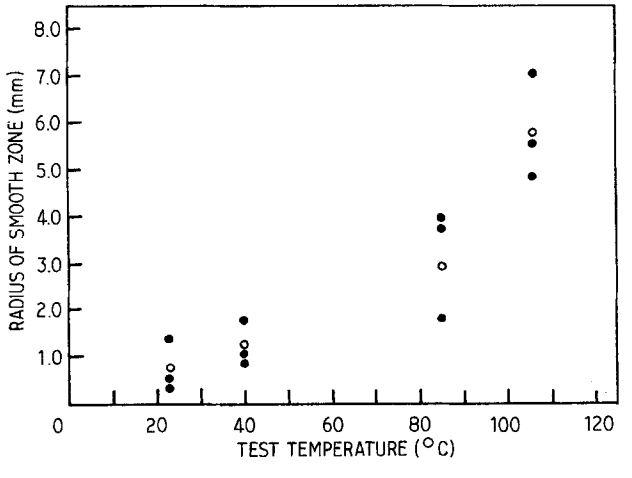


*Figure 11* The variation of the size of the smooth zone in the unfilled system with temperature: (○) signifies average.

a function of test temperature as shown in Fig. 11. Clearly, the dimensions of this region increase rapidly with increasing temperature until by 105° C it covers approximately 50% of the fracture surface.

### 3.2.2. Deformation mechanisms in the unfilled epoxy

Glassy polymers such as epoxy resins are generally considered to be brittle materials when tested at temperatures well below their glass transition. However, much evidence is now available to suggest that considerable local ductility and plastic flow can precede failure in these materials. Nevertheless, some disagreement still remains regarding the exact nature of this inelastic deformation. Morgan and O'Neal [8] claim to have identified craze-like structures around the origin of fracture in a highly cross-linked DGEBA epoxy.

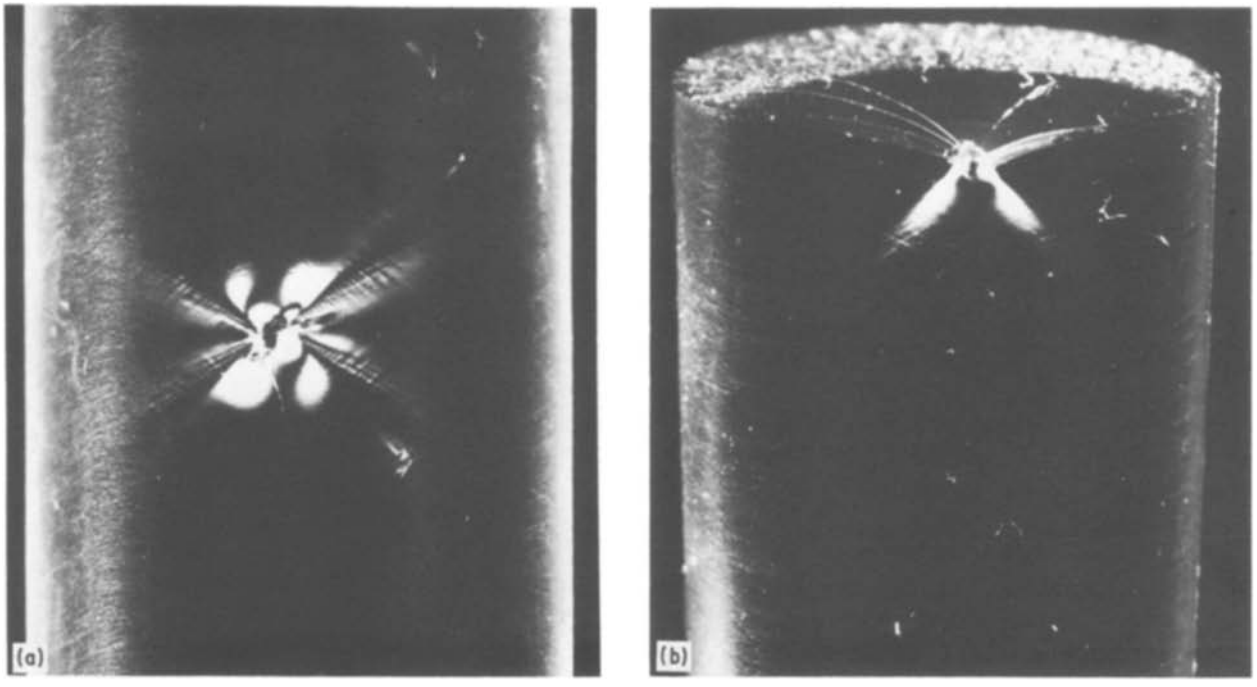


*Figure 12* Shear yielding in the unfilled epoxy system at elevated temperature: (a) shear bands at 85° C, (b) shear bands at 105° C. × 6.

The evidence presented is, however, not wholly conclusive since no clearly defined fibrils similar to those observed in many amorphous thermoplastics were found. It seems much more probable, therefore, that epoxides and other cross-linked materials deform through a shear yielding mechanism involving gross intramolecular motions. Glad [9], following an extensive programme of tests on epoxies with differing cross-link densities, concluded that shear yielding is indeed the primary mechanisms controlling fracture in such materials. Furthermore, he suggested that the effects observed by Morgan and O'Neal [8] were a result of stress concentrations due to defects, such as dust, in the thin films which were used for these investigations.

The evidence produced by the tests conducted here strongly substantiates the above view. Fig. 12 shows two specimens viewed under polarized light. In Fig. 12a two shear bands can be clearly seen extending away from a small defect at approximately 30°. Such bands can be seen to interact with the fracture surface in Fig. 12b, where the region of slow crack growth extends away from the intersection of the shear bands. Localized shear yielding of this type has also been observed near defects in specimens tested at room temperature, clearly demonstrating that the process of

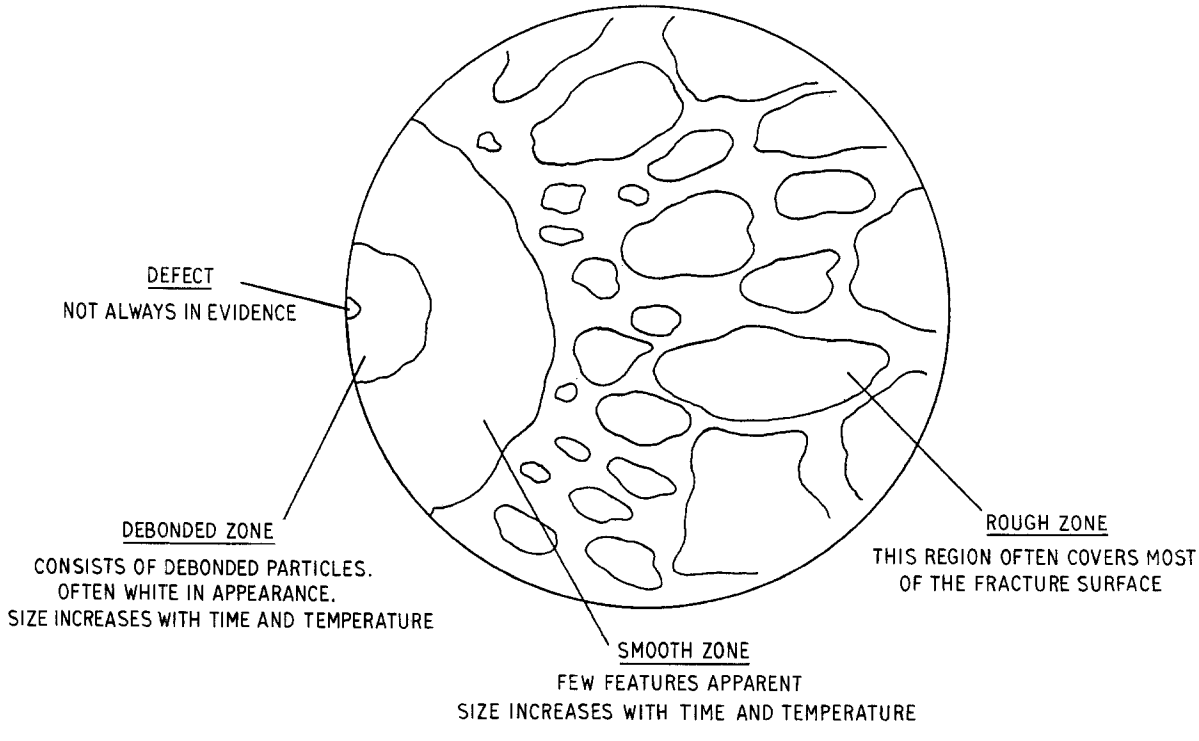


*Figure 13* Regions on the fracture surface in the filled epoxy.

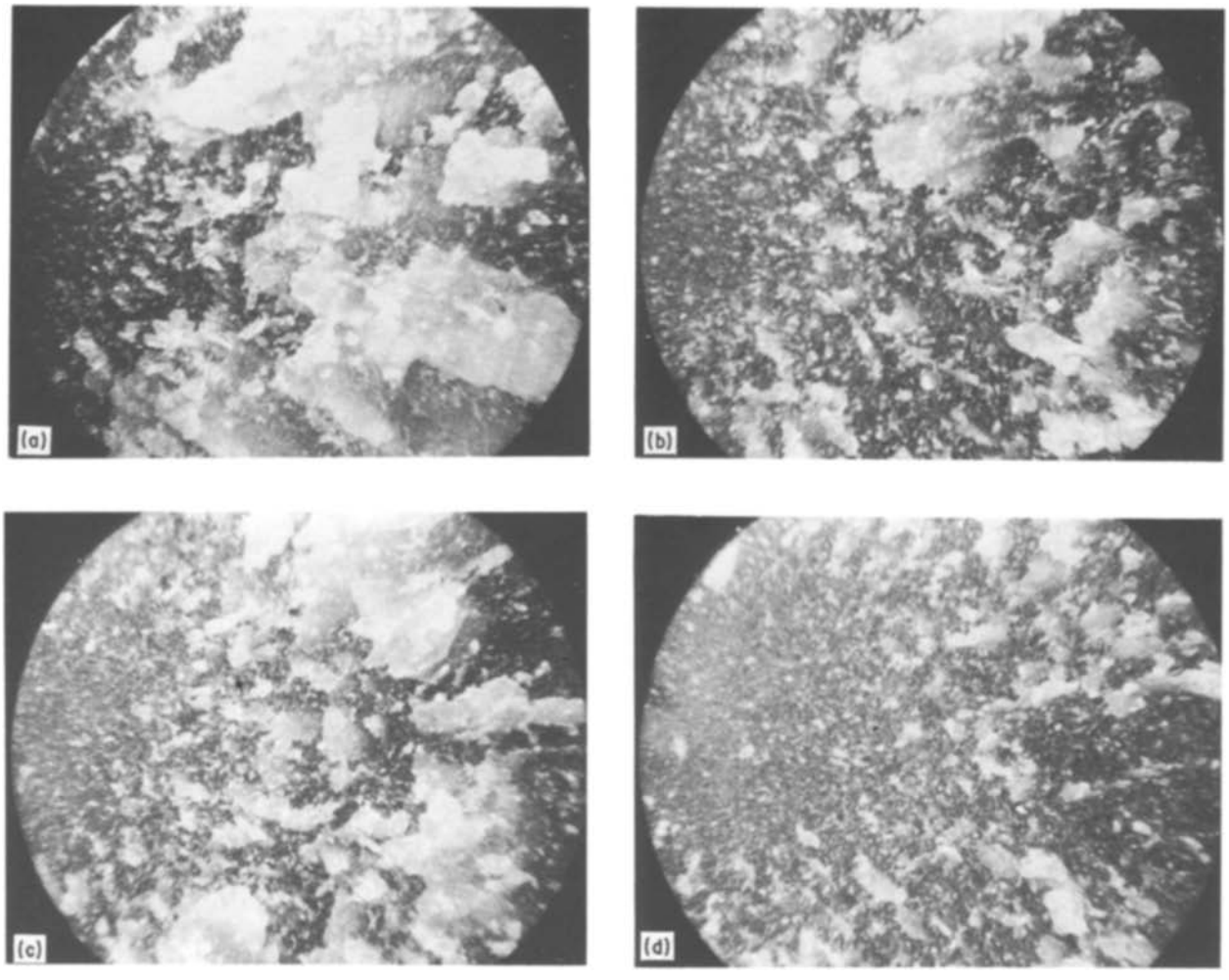


*Figure 14* Fracture surfaces in the filled epoxy as a function of temperature: (a) 23° C, (b) 50° C, (c) 85° C, (d) 105° C. × 6.

shear yielding represents the mechanism of inelastic deformation in this hydantoin-based epoxy resin.

### 3.2.3. The silica-filled resin

Fig. 13 presents a schematic diagram of the fracture surface of a typical filled resin. A cursory examination of these specimens highlighted four zones, the size and magnitude of which varied with the loading conditions and test temperature as shown in the optical micrographs given in Fig. 14. Fracture can sometimes be linked to the presence of a flaw or defect (Fig. 15a). The nature of these will be discussed in a subsequent section. The initiation point is surrounded by a region in which the particles are debonded from the matrix as shown in Fig. 15b. The size of this debonded region was found to increase rapidly with increasing

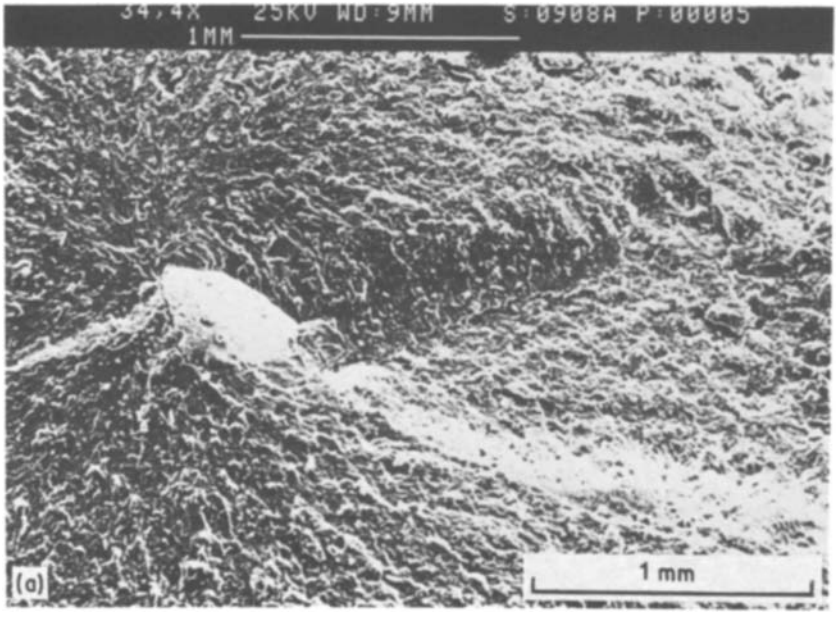


*Figure 15* Regions on the fracture surface in the filled epoxy: (a) defect, (b) debonded region, (c) smooth region at 50° C, (d) fast propagation region at 85° C.

*Figure 15* Continued.

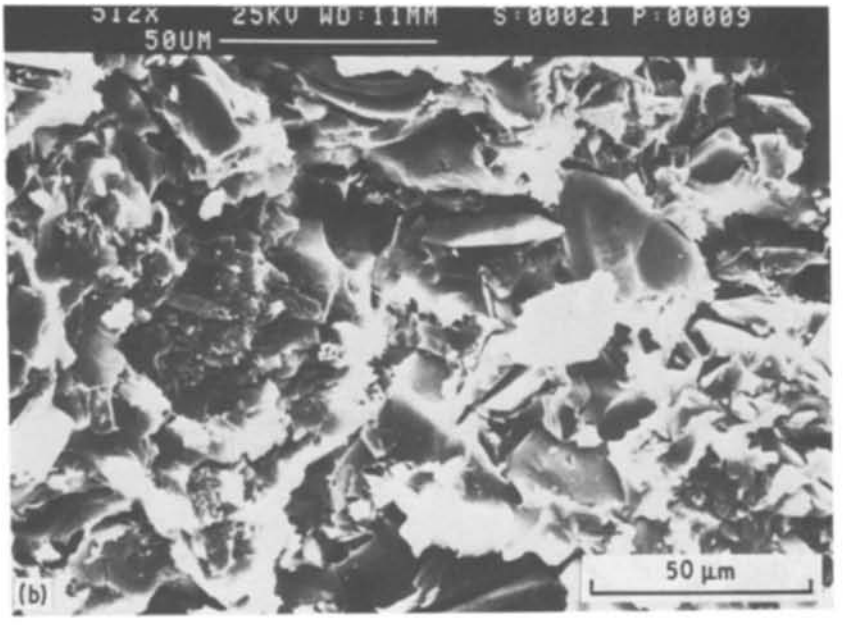


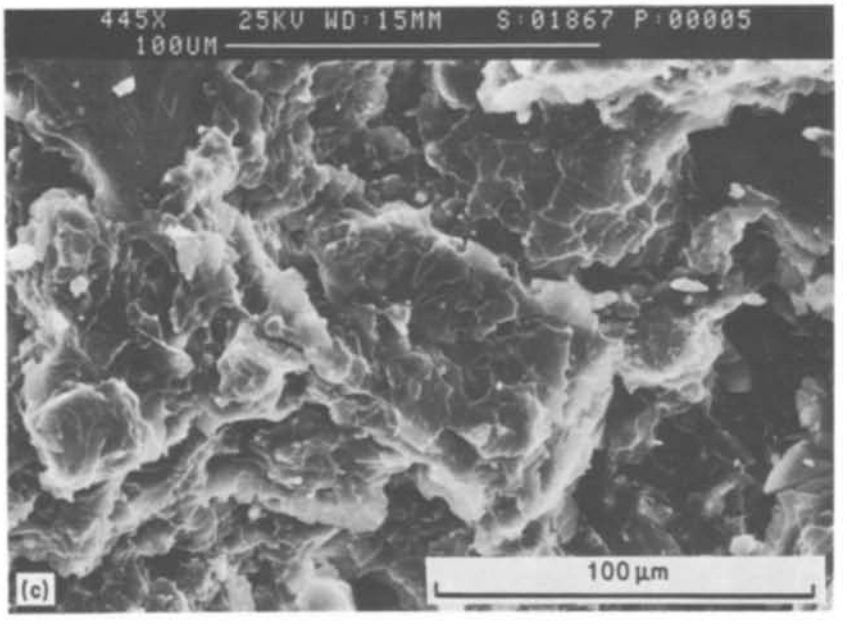


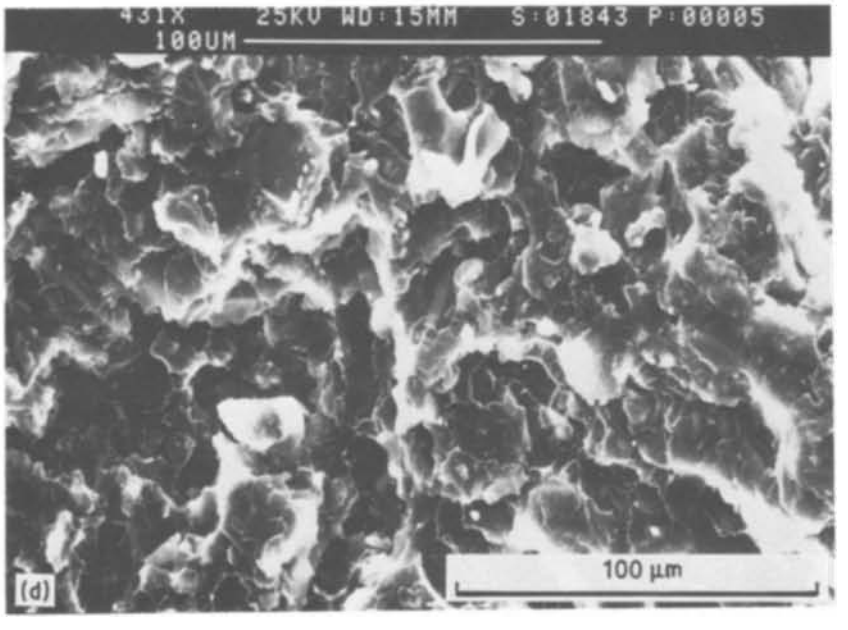

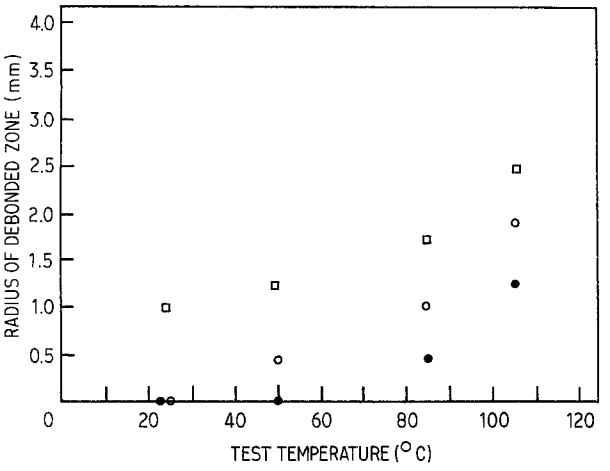


*Figure 16* The variation of the radius of the debonded zone with temperature and loading conditions: (●) strength test, (○) 80% ultimate, (□) 60% ultimate.

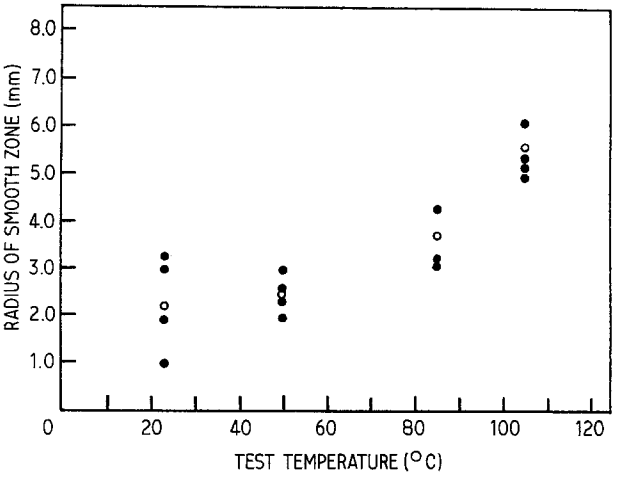


*Figure 18* The variation of the size of the smooth zone in the filled epoxy with temperature: (○) signifies average.

temperature and reducing load as shown in Fig. 16. In order to measure this debonded area, the specimens were gold-coated, using a sputtering machine which highlighted this zone (see Fig. 17), and then observed using an optical microscope. As a result, the size of this region was sometimes below the resolving power of the microscope (for example at high loads and low temperatures). Consequently, even though in such specimens the debonded area does have a finite size, it is necessary to plot these data on the $x$ axis in Fig. 16.

Beyond the debonded region is a smooth zone in which the particles are well bonded to the surrounding matrix (Fig. 15). However, unlike the unfilled epoxy this region cannot be linked to an area of slow crack growth. Here again, the size of this zone was dictated by the loading conditions and test temperature (Figs 18 and 19) and in certain cases can occupy a large percentage of the fracture surface. The remainder of the fracture surface exhibits a rough, strongly three-dimensional form indicative of rapid crack propagation and extensive crack branching. The extent of such crack branching was clearly determined by the conditions of test, being more severe in those specimens tested for short times at lower temperatures. The effects of creep loading on the fracture surface morphology is shown in Fig. 20, where three specimens tested at 23° C are presented. The specimen tested in a short-term test exhibits a small smooth zone with the majority of the fracture surface being occupied by the rough region where the effect of crack branching is clearly evident. With reducing load, the size of the smooth zone increases while the degree of crack branching reduces. At the time of writing, the specimens loaded at 20 and 40% of their ultimate strength have not yet broken, but previous unpublished work on creep specimens of square cross-section suggests that the surfaces will be almost entirely smooth displaying little, if any, crack branching.

Interestingly, when viewed macroscopically there is no significant difference between specimens which, although tested under the same conditions (load level and temperature), have failed at different strain levels and time intervals. This is demonstrated in Fig. 21 where two specimens tested at 85° C and 60% ultimate load are presented. Closer examination shows there is no distinct macroscopic difference between the two fracture surfaces although their conditions of failure were substantially different. The elastic energy stored at fracture was identical for the two samples, that is 0.92 J. (Since the time under load differed, the size of the debonded zones were not, however, the same.)

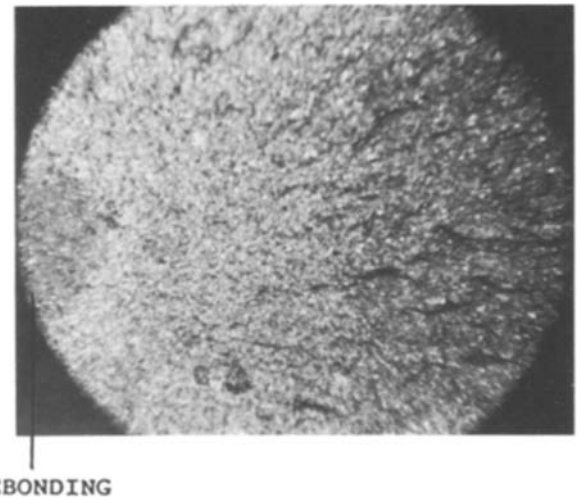


*Figure 17* An optical micrograph of a specimen tested at 85° C showing the regions of debonding. × 6.

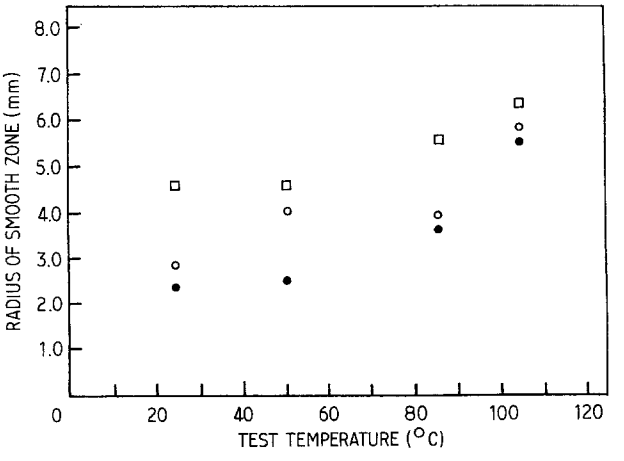


*Figure 19* The variation of the size of the smooth zone in the filled epoxy with temperature and loading: (●) strength test, (○) 80% ultimate, (□) 60% ultimate.

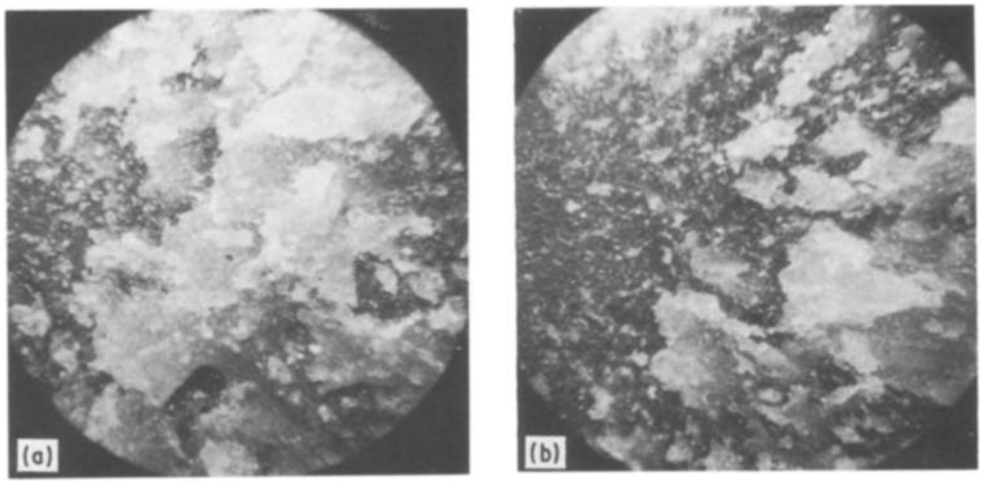


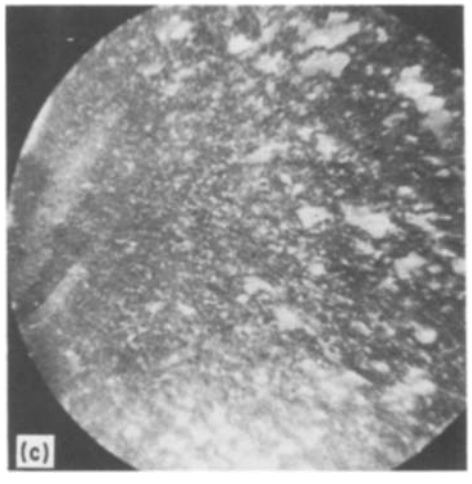


*Figure 20* The effect of loading conditions on fracture surface morphology: (a) strength test, (b) 80% ultimate, (c) 60% ultimate. × 5.

### 3.2.4. Deformation mechanisms in the filled epoxy resin

Based on observations under polarized light, it was possible to establish that shear yielding was the primary mechanism of inelastic behaviour in the unfilled epoxy system. However, conducting similar tests with the filled epoxy is more difficult due to the non-transparent nature of this system. There is, however, strong evidence to suggest that shear yielding is also the primary mechanism in this filled resin. Fig. 22 shows a specimen tested at 60% ultimate load and at 105° C. Here two intersecting stress-whitened bands extending at approximately 45° can be clearly seen. The possible causes of this stress-whitening will be discussed elsewhere [10]; however, this evidence strongly suggests that this mechanism is linked to the inelastic deformation associated with shear yielding and resin–particle debonding. Recent work, using polished thin sections, has clearly shown the existence of shear bands in specimens deformed in tension and compression [10].

## 3.3. Identification of the regions on the fracture surface

The following section will attempt to examine and explain the causes and possible consequences of the different regions on the fracture surface. Attention will be focused on the filled system although reference will be made, where necessary, to effects noted in its unfilled counterpart.

### 3.3.1. The defect

Defects initiating fracture may arise for many reasons, and several possibilities are listed below.

*3.3.1.1. Specimen preparation.* Defects associated with the preparation of test samples and large-scale parts

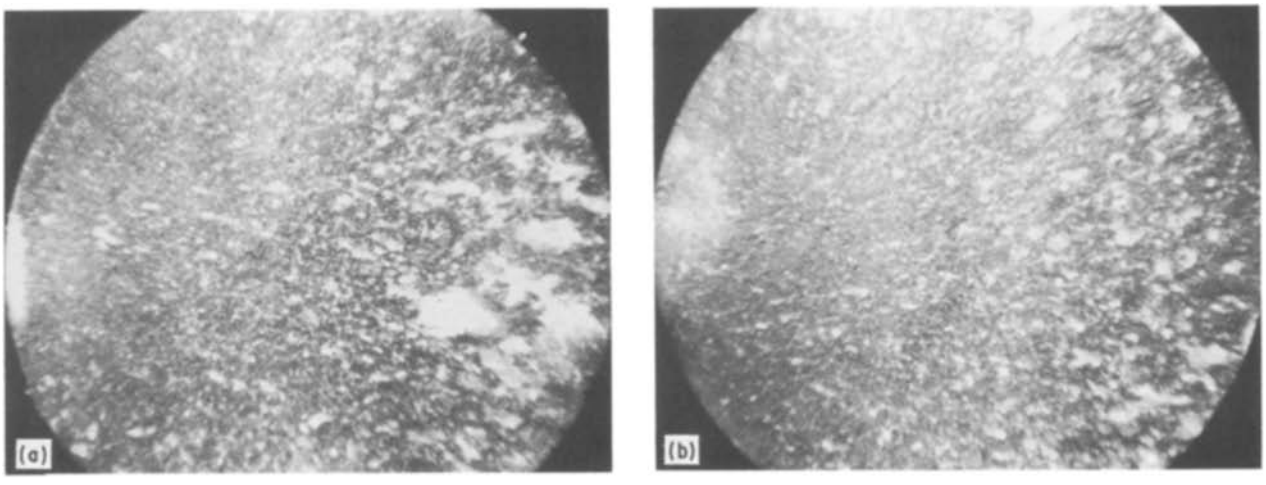


*Figure 21* Two optical micrographs showing the effect of long-term loading on fracture surface morphology; loading 60% ultimate, temperature 85° C. (a) Failure strain 0.81%, failure time 1.3 × $10^5$ sec; (b) failure strain 1.03%, failure time 6.5 × $10^5$ sec.

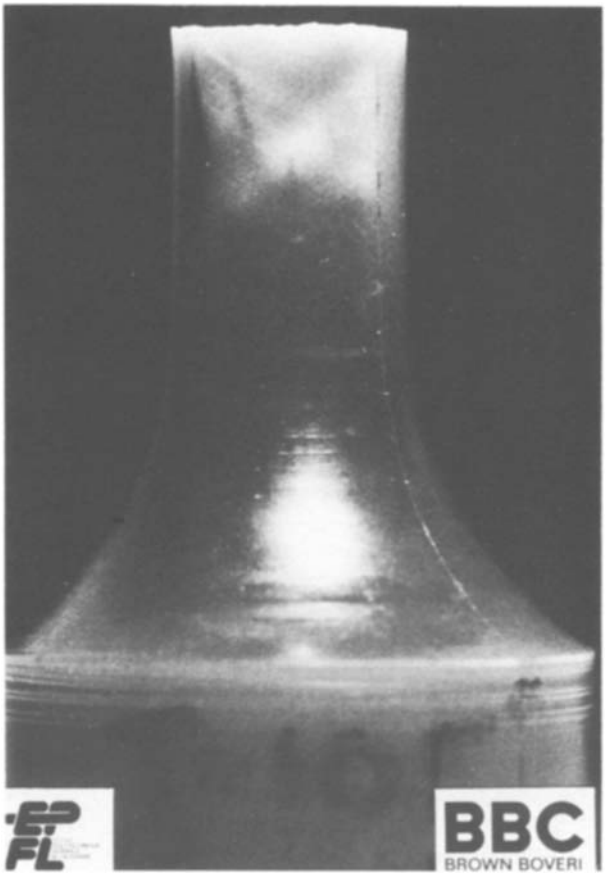


*Figure 22* Evidence of shear yielding in the filled epoxy system; loading 60% ultimate; temperature 105° C.

include air bubbles, resin-rich areas, mould lines and foreign matter such as dust particles.

*3.3.1.2. Particle size.* Previous calculations of effective inherent flaw sizes in silica-filled epoxy resins yielded values of the order of 100 $\mu$m [7], suggesting the presence of particles significantly larger than the mean size (typically 50 $\mu$m). Subsequent SEM analyses have indeed identified particles of this size, suggesting that they might be a cause of fracture in such systems.

*3.3.1.3. Poorly bonded or weak particles.* Previous work has shown [7] that the large flaw sizes determined for untreated alumina composites (290 $\mu$m) probably derive from the linking-up of weakly bonded particles at relatively low levels of stress. The flaw sizes of composites prepared from alumina trihydrate were in the range 300 to 500 $\mu$m. Since these particles are relatively weak it was suggested that the flaw was generated during the test as they fractured under the increasing load [7].

### 3.3.2. The debonded zone

The size of the debonded region surrounding the point of initiation is of particular interest, as its size appears to be a crucial parameter in controlling the static fatigue lifetime of these materials. At a given temperature, the size of this zone increases with time of loading (Fig. 23). These dimensions were determined, as before, by direct observation of the gold-coated sample under the optical microscope following fracture under creep loading. The appearance of such debonded regions suggested that this mechanism was linked to some form of slow, sub-critical crack growth similar to that observed in the unfilled epoxy. In order to examine this possibility in more detail, a series of double-torsion tests was conducted over a temperature range of 23 to 105° C. The advantage of such a test lies in the fact that the double-torsion geometry is essentially stable, enabling crack velocities as low as $10^{-6}$ m sec$^{-1}$ to be achieved quite easily. Two examples of the resulting fracture surfaces are shown in Fig. 24. In both cases it is evident that the particles are totally separated from their neighbouring matrix in a manner similar to that observed in the dumb-bell specimens discussed above. The information from this series of tests is presented in graphical form in Fig. 25, where the variation of the debonding threshold is determined as a function of test temperature. On examining this curve, it is clear that particle–matrix separation can occur at all temperatures considered. However, the velocity at which debonding begins is strongly temperature-dependent; at 105° C debonding is apparent over the whole span of crack velocities. In order to analyse further the causes and resulting effects of particle debonding, a fracture mechanics type of analysis was conducted where the stress at failure $\sigma_f$ is related to the debonded zone size ($a$) by the relationship

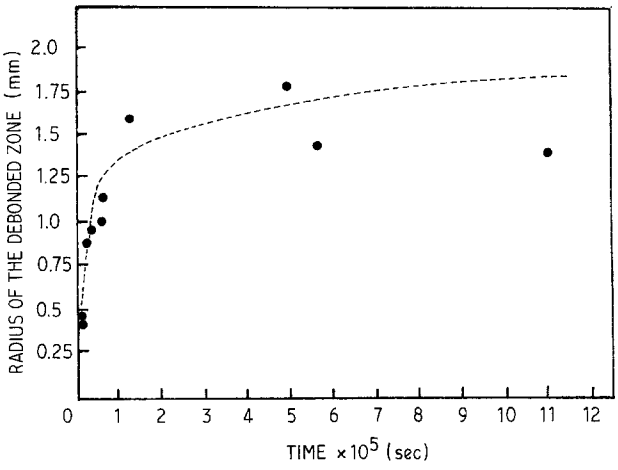


*Figure 23* The variation of the size of the debonded zone with time at 85° C.

$$K_{Ic} = \sigma Y a^{1/2}$$

where $K_{Ic}$ is the fracture toughness and $Y$ is a geometric factor taken here as the value for an edge-notch in an infinitely wide sheet. Fig. 26 shows that the data comply reasonably well with the trends predicted by linear elastic fracture mechanics, and a value for the fracture toughness of 2.29 MPa m$^{1/2}$ was determined by a curve fitting procedure. This value is in quite good agreement with the value determined previously for this material [11].

The evidence presented above substantiates the suggestion that the debonded zone represents the region where the crack grows slowly and sub-critically. It is reasonable to assume, therefore, that this region will be critical in determining the static fatigue resistance of such a composite component.

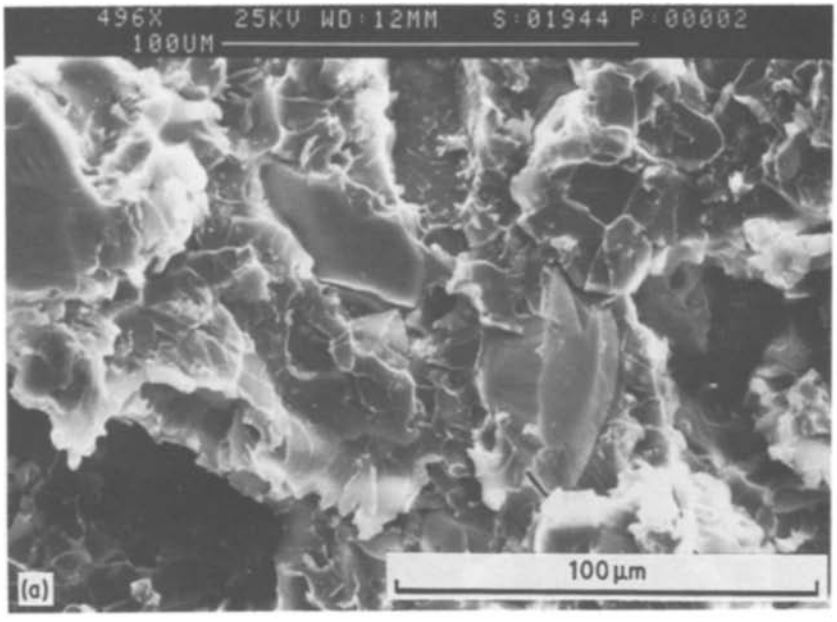


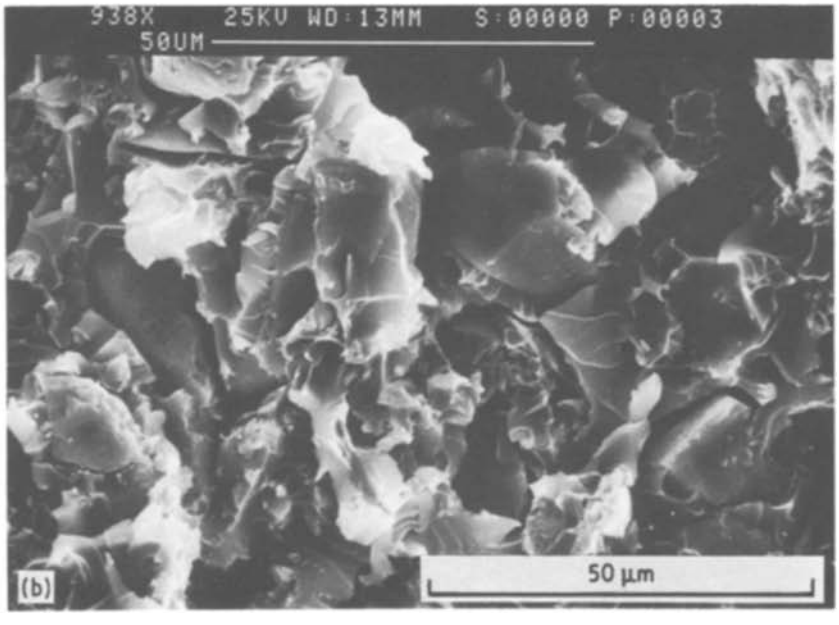


*Figure 24* Double-torsion specimens showing particle–matrix debonding: (a) temperature 23° C, velocity $5.3 \times 10^{-6}$ m sec$^{-1}$; (b) temperature 85° C, velocity $4.2 \times 10^{-6}$ m sec$^{-1}$.

### 3.3.3. The smooth zone

The smooth zone is a relatively flat, featureless region surrounding the initiation and debonded zone whose size increases rapidly with increasing test temperature and decreasing applied load.

It has already been suggested that the crack velocity in this region is high; indeed, there is certainly no evidence to link this zone with the slow-growth mirror region observed in the unfilled system. Physically determining the crack velocity in this region is extremely difficult since the geometry of the dumb-bell specimen is not conducive to the use of the graphite gauge. Instead, testing was conducted on the single-edge notch geometry in which the crack velocity can be readily determined. Fig. 27 shows a typical crack length against time profile and subsequent velocity against time curve for one such test. The sensitivity and flexibility of the data recorder permit the crack velocity to be determined accurately at any point on the fracture surface. In Fig. 28 the fracture surface of a single-edge-notch specimen is given together with the corresponding velocity profile. Closer examination of the figure highlights the pre-crack on the immediate left of the specimen (0.25 mm), followed by a smooth region similar in appearance to that noted in the previous dumb-bell specimens. Further away from the point of fracture initiation the surface becomes very rough and three-dimensional with many large whitened features indicative of crack branching. The corresponding velocity profile indicates that over the smooth zone the crack is continuously accelerating, and only when it achieves its maximum value (800 m sec$^{-1}$) does the fracture surface exhibit the previously discussed roughness. This suggests, therefore, that the smooth region in this filled epoxy corresponds to the region of crack acceleration in which all excess energy is dissipated by driving the crack faster. When the crack reaches its terminal value (800 m sec$^{-1}$ in this material) any excess energy must now be dissipated in another manner, namely by crack branching.

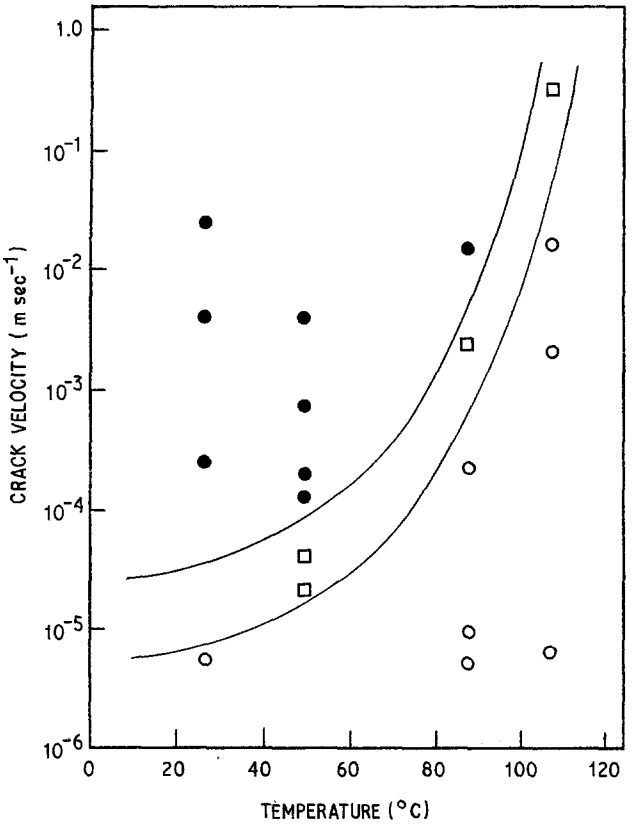


*Figure 25* The effect of crack velocity on particle–matrix debonding (double-torsion geometry). (●) Well-bonded, (□) partially bonded, (○) debonded.

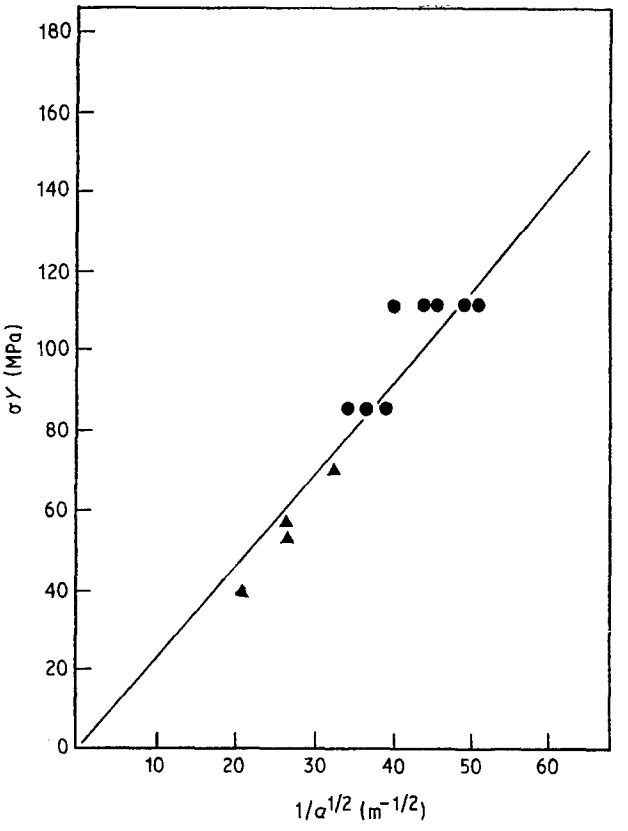


*Figure 26* Fracture mechanics correlation for (●) creep tests at 85° C, and (▲) single-edge-notch tests, at 85° C. Slope = 2.29 MPa $m^{1/2}$.

### 3.3.4. The rough region

Surrounding the smooth, featureless zone in these filled epoxy resins is a rough zone whose whitened, three-dimensional appearance is indicative of high-velocity crack branching. Fig. 29 gives clear evidence of this phenomenon where the side faces of a single-edge-notch specimen and a rectangular-section tensile specimen are shown. Branching of rapidly propagating cracks in glass was recorded some time ago by Schardin [12], and since then other workers observed similar effects in both fully crystalline and amorphous materials [13, 14].

Crack branching has not been explained successfully by analytical methods since the equations of linear elasticity must be solved independently from the constitutive (non-linear) equations of deformation. Instead, most explanations stem from simple mechanical models or semi-empirical analyses. Yoffe [15] attempted to explain dynamic crack branching by considering a crack of constant length propagating across an infinite medium. It was found that the maximum circumferential stress acted normal to the lines inclined at 60° to the crack front. The action of such stresses was believed to be adequate to create a condition for the rapidly propagating crack to bifurcate. More recently, a number of severe discrepanceis have been found in this analysis which, although attractive due to its simplicity, is clearly invalid. Ravi-Chandar and Knauss [16] suggest that crack branching is a process controlled by the formation of voids ahead of the unstable primary crack. They propose that when the stress intensity factor of the crack reaches a critical value, an array of voids and cavities forms in the locally high stress concentrations creating an "ensemble" crack front and the necessary condition for branching.

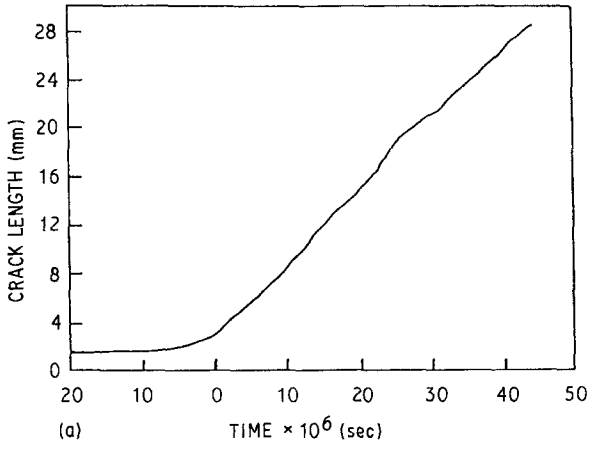


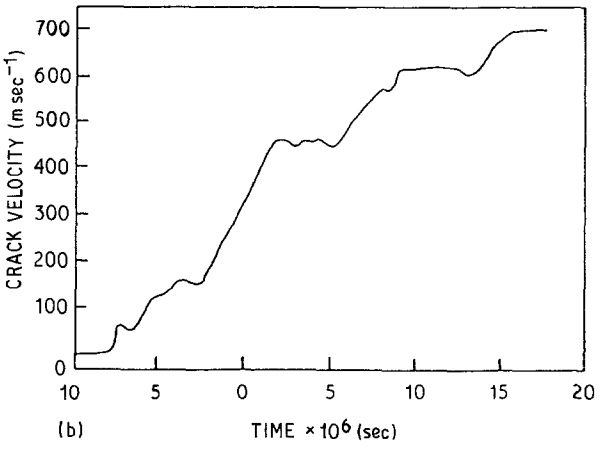


*Figure 27* Crack extension in a filled single-edge-notch specimen: (a) crack length, (b) crack velocity.

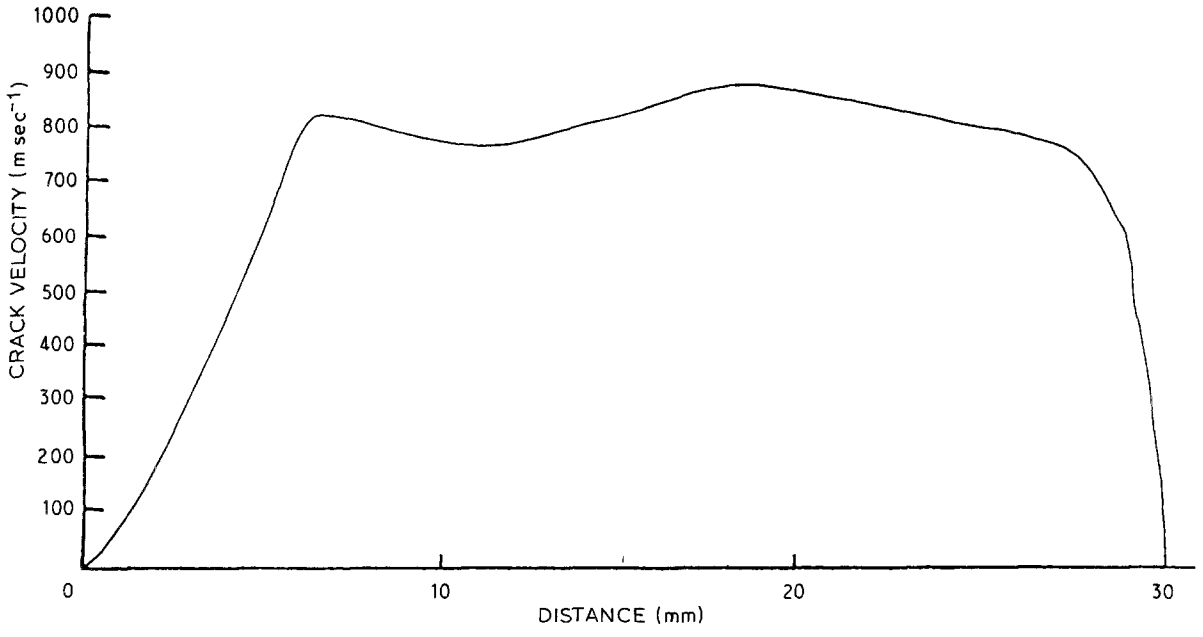


*Figure 28* The variation of crack velocity across the surface of a single-edge-notch specimen in the silica-filled resin. × 7.

Johnson and Hollaway [17] as well as Bansal [18] have attempted to explain crack branching by considering the rate of supply of energy to the tip of the propagating crack. They claim that separation of the crack front occurs when this energy supply rate becomes excessive, the creation of multiple fracture surfaces being the only means of assuring its complete dissipation. Eshelby's approach [19] is also based on an energy criterion, proposing that branching occurs at a crack velocity of 0.3 times the shear wave velocity, once again due to an excessive supply of energy to the rapidly propagating crack front.

We also believe that an energy supply criterion is sufficient to explain the phenomena of dynamic crack branching. The amount of elastic energy stored in the specimen at the moment of fracture may be determined from the area under the stress-strain curve at rupture, that is

$$U = \int \frac{\sigma^2}{2E} \, dv$$

where $\sigma$ is the applied stress, $E$ is Young's modulus and $v$ is the volume under load. Fig. 30 shows the fracture surfaces of a series of specimens tested at various temperatures for short and long times. In the upper left-hand corner is a specimen which had undergone a strength test (failure time 5 min) at 23° C and intermediate samples represent strength tests at higher temperatures and creep tests at room temperature. Finally in the lower right-hand corner is a creep sample at 105° C which was under load for 1000 h. Under each sample is given the amount of energy stored in the specimen (in joules) at the moment of fracture. It can be seen from Fig. 30 that qualitatively

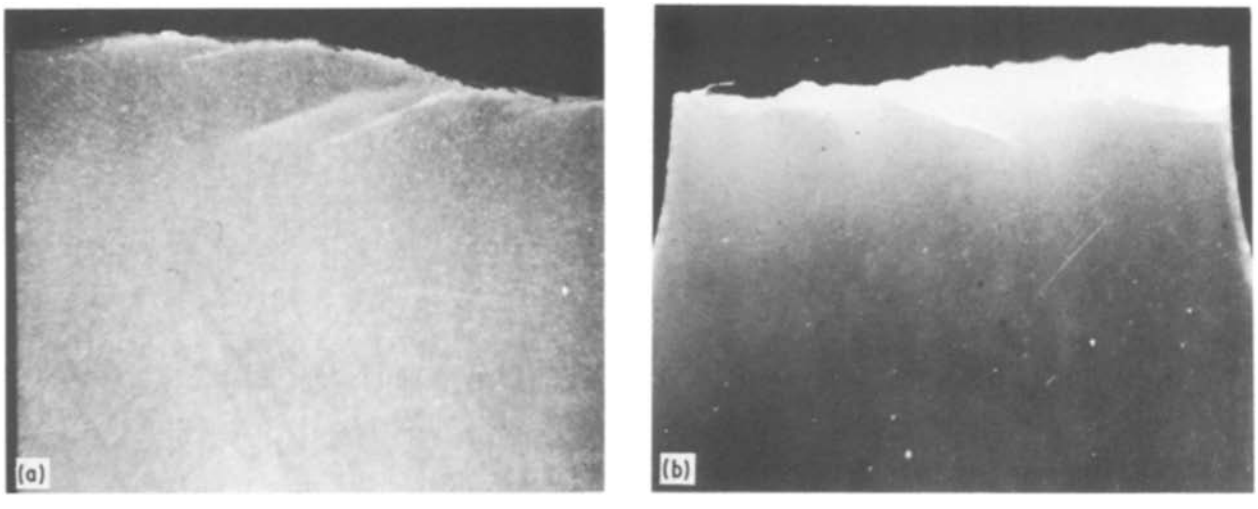


*Figure 29* Examples of crack branching in the filled epoxy system: (a) single-edge-notch at 85° C, (b) tension specimen at 23° C. × 7.

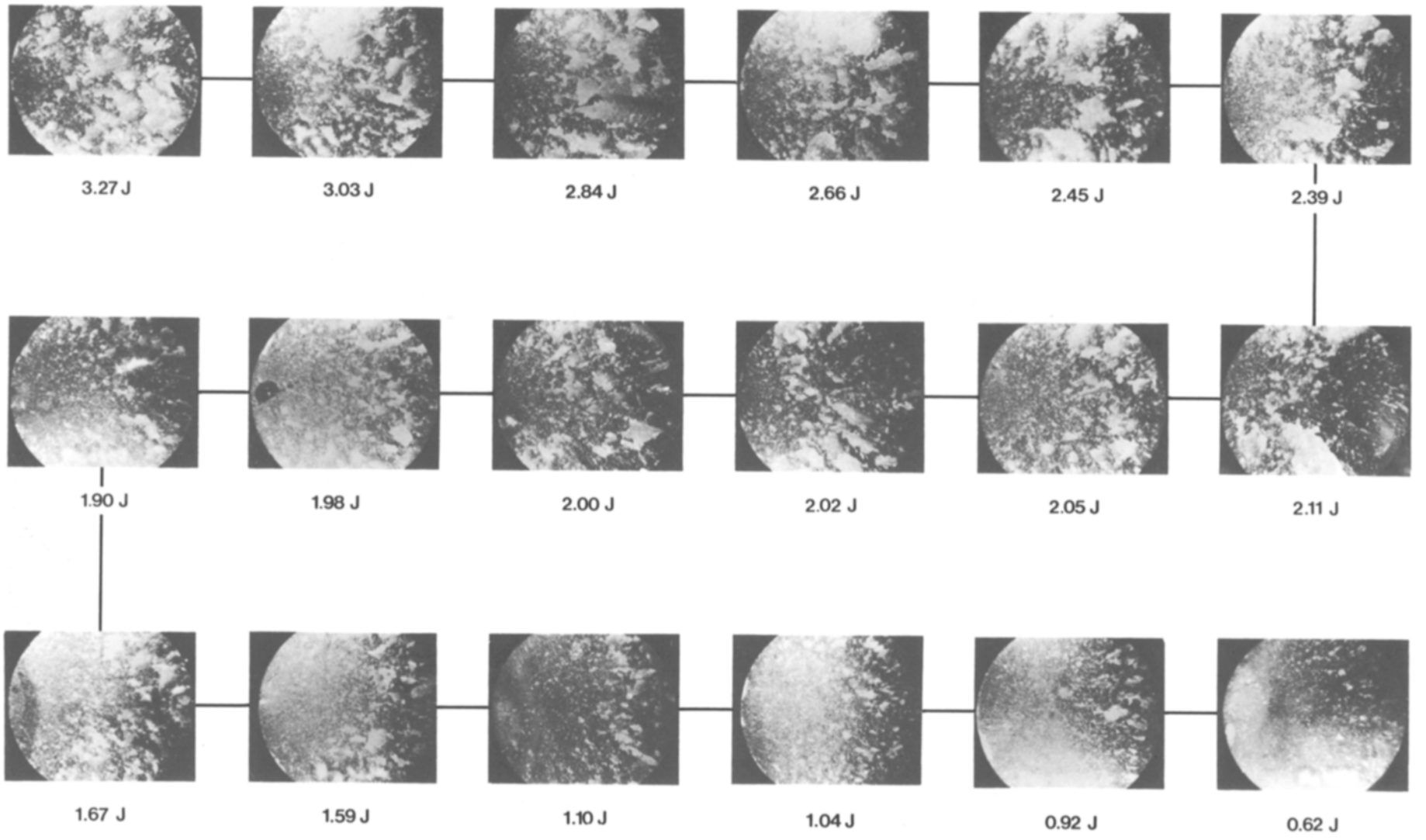


*Figure 30* Relationship between fracture surface morphology and stored elastic energy.

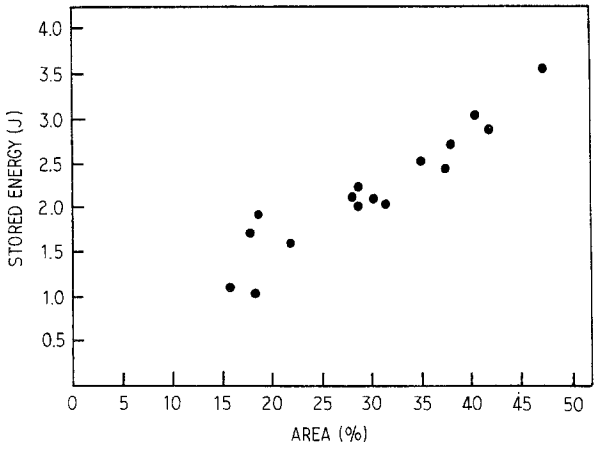


*Figure 31* The use of the image analyser to characterize the fast fracture surface.

this energy correlates well with the surface roughness. Since the brightness of the fracture surface is governed by the amount of crack branching sustained, those specimens failing with greater stored elastic energy reflect more light. An attempt was made to quantify these effects using an image analyser (interactive image analysis system IBAS made by Kontron, West Germany). Here the photographs of the fracture surfaces, as shown in Fig. 30, were placed above the analysing camera enabling a two-tone image of the fracture surface to be recorded. A supporting computer system was then employed to determine the relative percentages of bright and dark regions on the fracture surface, enabling a quantitative analysis to be made of the wide range of samples with differing thermo-mechanical histories. In Fig. 31 the percentage of surface whitening ($A$) is plotted as a function of the stored elastic energy for each specimen ($U$). The figure clearly identifies a unique, linear correlation between $U$ and $A$ over the whole range considered.

Thus at points where the crack velocity is below its limiting value all excess energy can be dissipated by accelerating the crack further. When this limiting velocity is achieved any superfluous energy must now be expended in creating multiple fracture planes and thus increasing the surface roughness.

## 4. Conclusions

1. The fracture surfaces of the silica-filled epoxy resin can be characterized by four regions:

(a) defect (although not always in evidence),
(b) a debonded region,
(c) a smooth zone,
(d) a rough zone.

2. The debonded region represents the zone of sub-critical growth, the development of which controls the static fatigue lifetime.

3. The smooth zone corresponds to the area over which the crack is accelerating. Here it seems that the excess energy is dissipated in driving the crack faster.

4. The rough region occurs when the crack velocity has attained its limiting value, here all excess stored elastic energy is dissipated in creating new fracture surfaces by crack branching.

5. Using an optical photo-microscope and an image analyser it is possible to quantify many of the features apparent on the fracture surface of filled epoxy systems.

## Acknowledgements

The authors would like to thank Professor H. H. Kausch for his continued support and encouragement and Brown Boveri & Cie and the Commission pour l'Encouragement de la Recherche Scientifique for the financial assistance which made this project possible. They would also like to thank Brian Senior and the Institut Interdepartmental de Microscopie (EPFL) for much help with scanning electron microscopy, Jean-Luc Roulin for technical assistance and J. W. Smith, H. R. Beer and A. Demarmels (BBC) for helpful suggestions and discussions.

## References

1. B. ROSEN (ed.), "Fracture Processes in Polymeric Solids: Phenomena and Theory" (Interscience, New York, 1964).
2. B. W. CHERRY and K. W. THOMSON, *J. Mater. Sci.* **16** (1981) 1925.
3. M. J. OWEN and R. G. ROSE, *ibid.* **10** (1975) 1711.
4. B. E. NELSON and D. T. TURNER, *Polym. Lett.* **9** (1971) 677.
5. C. B. BUCKNALL, "Toughened Plastics" (Applied Science, London, 1977).
6. B. STALDER, Ph. BÉGUELIN and H. H. KAUSCH, *Int. J. Fracture* **22** (1983) R47.
7. A. C. MOLONEY, H. H. KAUSCH, T. KAISER and H-R. BEER, *J. Mater. Sci.* **22** (1987) 381.
8. R. J. MORGAN and J. E. O'NEAL, *ibid.* **12** (1977) 1966.
9. M. GLAD, PhD thesis, Cornell University (1986).
10. J. W. SMITH, T. KAISER and A. C. ROULIN-MOLONEY, *J. Mater. Sci.*, submitted.
11. H-R. BEER, T. KAISER, A. C. MOLONEY and H. H. KAUSCH, *J. Mater. Sci.* **21** (1986) 3661.
12. H. SCHARDIN, in "Fracture", edited by B. L. Averbach, D. K. Felbeck, G. T. Hahn and D. A. Thomas (Wiley, New York, 1959) p. 297.
13. J. P. DEMPSEY and P. BURGERS, *Int. J. Fracture* **27** (1985) 203.
14. Z. T. BIENIAWSKI, *ibid.* **4** (1968) 415.
15. E. H. YOFFE, *Phil. Mag.* **42** (1951) 739.
16. K. RAVI-CHANDAR and W. G. KNAUSS, *Int. J. Fracture* **26** (1984) 141.
17. J. W. JOHNSON and D. G. HOLLOWAY, *Phil. Mag.* **14** (1966) 731.
18. G. K. BANSAL, *ibid.* **35** (1977) 935.
19. J. D. ESHELBY, in "Inelastic Behaviour of Solids", edited by M. F. Kanninen, W. Alder, A. Rosenfield and R. Jaffe (McGraw-Hill, New York, 1970) p. 111.

*Received 8 May*
*and accepted 22 July 1987*